HIGH RESOLUTION NEUTRON SPECTROSCOPY IN THE KILOVOLT REGION

by

Paul Frothingham Nichols

Department of Physics
Duke University

Date: May 8 1957

Approved:

Henry W. Newson

Henry W. Newson, Supervisor

Walter Ford

J. M. Blatt

Eugene Gluekauf

F. D. Seward

A dissertation submitted in partial fulfillment of the requirements for the degree of Doctor of Philosophy in the Department of Physics in the Graduate School of Arts and Sciences of Duke University

1958

CONTENTS

LIST OF FIGURES

HIGH RESOLUTION NEUTRON SPECTROSCOPY IN THE KILOVOLT REGION

Chapter I

INTRODUCTION

Since the discovery of the neutron by Chadwick[1] in 1932, there has been a rather large amount of interest, both theoretical and experimental, in the interaction between neutrons and atomic nuclei. In the 1930's considerable theoretical progress was made by Bohr,[2] Breit and Wigner,[3] and others. These theories predicted the occurrence of resonances and much experimental work has been done in the measurement of these resonances. Neutron energy determinations and resolution have increased greatly since the experiments of Fermi et al[4] and Dunning and Pegram[5] in the 1930's. Such techniques as the use of reactors in conjunction with neutron velocity selectors and neutron crystal spectroscopy have been developed. Such methods are suitable for measurements in the electron volt region and have been refined to a high degree. Of particular interest with reference to this report has been the development of nearly monoenergetic

neutron sources through the utilization of charged particle reactions which produce neutrons. One very successful combination is the use of a Van de Graaff to accelerate protons which impinge upon a lithium target and then produce neutrons from the endoergic Li(p,n) reaction. The development of a neutron spectrometer which is capable of high resolution measurements is reported in this thesis. Some measurements are presented which have been made with the instrument using the Li(p,n)Be reaction as a neutron source. The spectrometer has resolved some previously unreported resonances and has measured others with a higher degree of resolution than has been obtained before. High resolving power enables one to determine the parameters of a resonance more accurately and also to resolve resonances which previously appeared to be overlapping.

Bi^{209} was selected as the nucleus to be investigated with the new spectrometer in the region from 10 to 135 kev. Although the level spacing increases with atomic number in general and is so small that the resonances are actually overlapping for most heavy nuclei in this energy range, bismuth which has a "magic" number of neutrons and nearly a "magic" number of protons exhibits an unusually large level spacing as do other nuclei with magic or near magic numbers of neutrons or protons. The levels in bismuth are quite narrow and are therefore an interesting subject for high resolution investigation.

Let us look briefly at the Breit-Wigner[6] single level formula which describes isolated resonances. We shall consider only the case for s-wave neutrons because all the resonances

observed in this experiment appear to have the characteristic interference dip of such resonances. A brief derivation is included in Appendix A. The final result is as follows:

$$\sigma_{sc} = g_1 \pi \lambda^2 \left| A_{res} + A_{pot} \right|^2 + (1 - g_1) \pi \lambda^2 \left| A_{pot} \right|^2$$

where g is the statistical weight factor for the resonant channel, λ is the incident neutron de Broglie wavelength, and A_{res} and A_{pot} are complex resonance and potential scattering amplitudes. This expression exhibits a minimum value for an energy slightly less than resonance, and a maximum at an energy slightly greater than resonance. The value of the cross section also decreases less rapidly from its maximum value when the energy is increasing than when it is decreasing. In essence one compares the experimentally determined cross section with the theoretical cross section, both with regard to shape and peak height. In the laboratory a count is made for a given neutron flux first with the detector shadowed by a sample of the element under investigation, and secondly with the detector unshadowed. This measurement is performed as a function of neutron energy. The experimentally determined apparent total cross section is related to the transmission ratio, T, by the exponential expression, $T = \exp(-N\sigma)$ where N is the sample thickness. This cross section is in general subject to correction; the true cross section is usually larger.

Chapter II

DESCRIPTION OF EQUIPMENT

The proton beam (see Figure 1) from the Van de Graaff electrostatic accelerator is passed through a magnetic analyzer and then into a modified cylindrical electrostatic analyzer[7] before it goes into the neutron spectrometer. The modification[8] of the electrostatic analyzer is discussed later. The beam passes through a one inch stainless steel tube which runs directly through the instrument and impinges upon a lithium target evaporated onto a .001 inch tantalum backing. The spectrometer itself (see Figure 2) consists of three polyethylene cones which are all coaxial with the beam tube. The cones focus upon the Li target and define a collimator for the neutrons which are emitted at laboratory angles of between 160° and $160^{\circ} + \Delta\theta$ where $\Delta\theta$ is the angular opening. The first cone (Cone A, Figure 2) has a female inner conical surface and has a cubic outer configuration. This cone is stationary. The second truncated cone

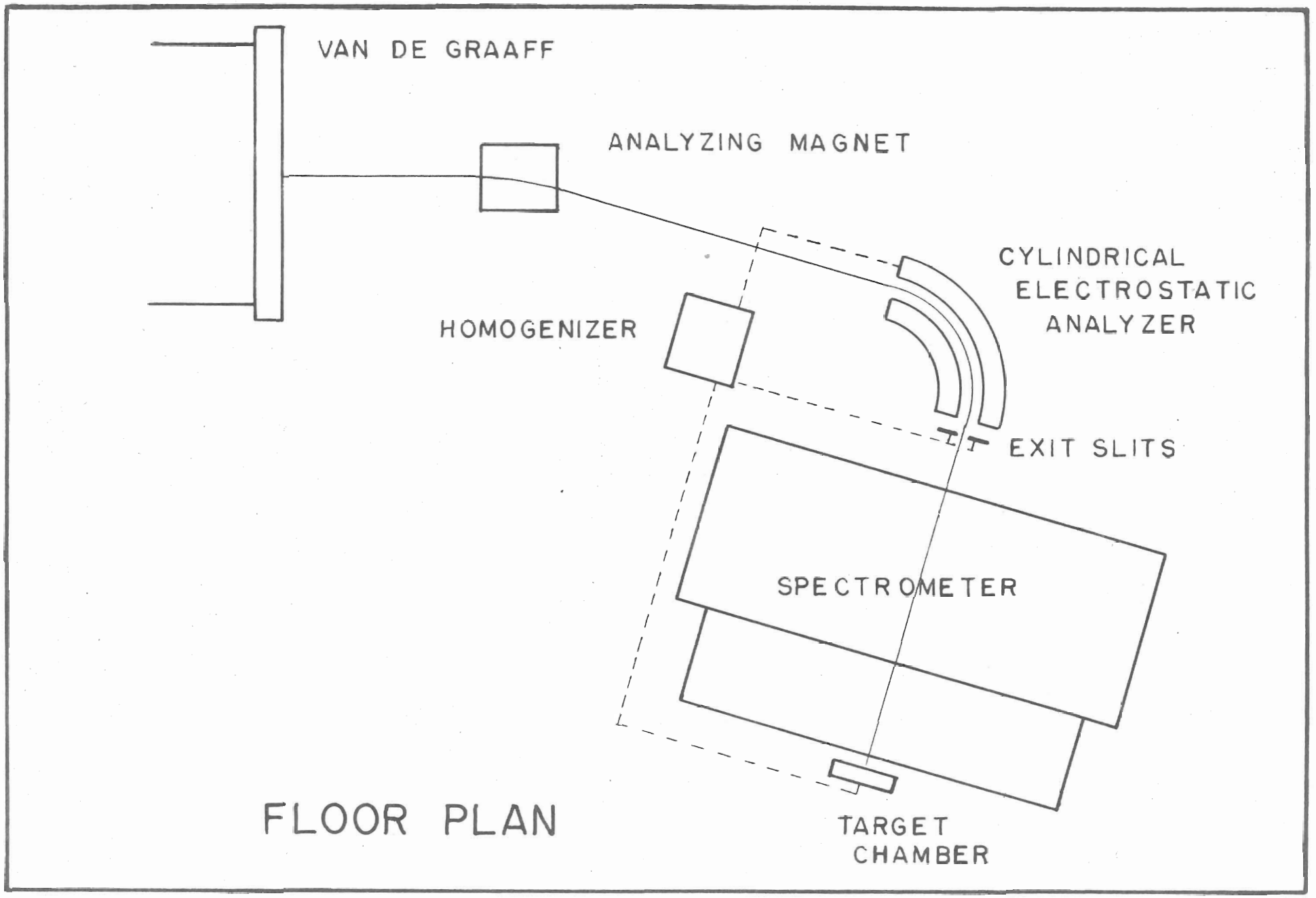

Figure 1. Relative Position of Major Components in the Duke Laboratory

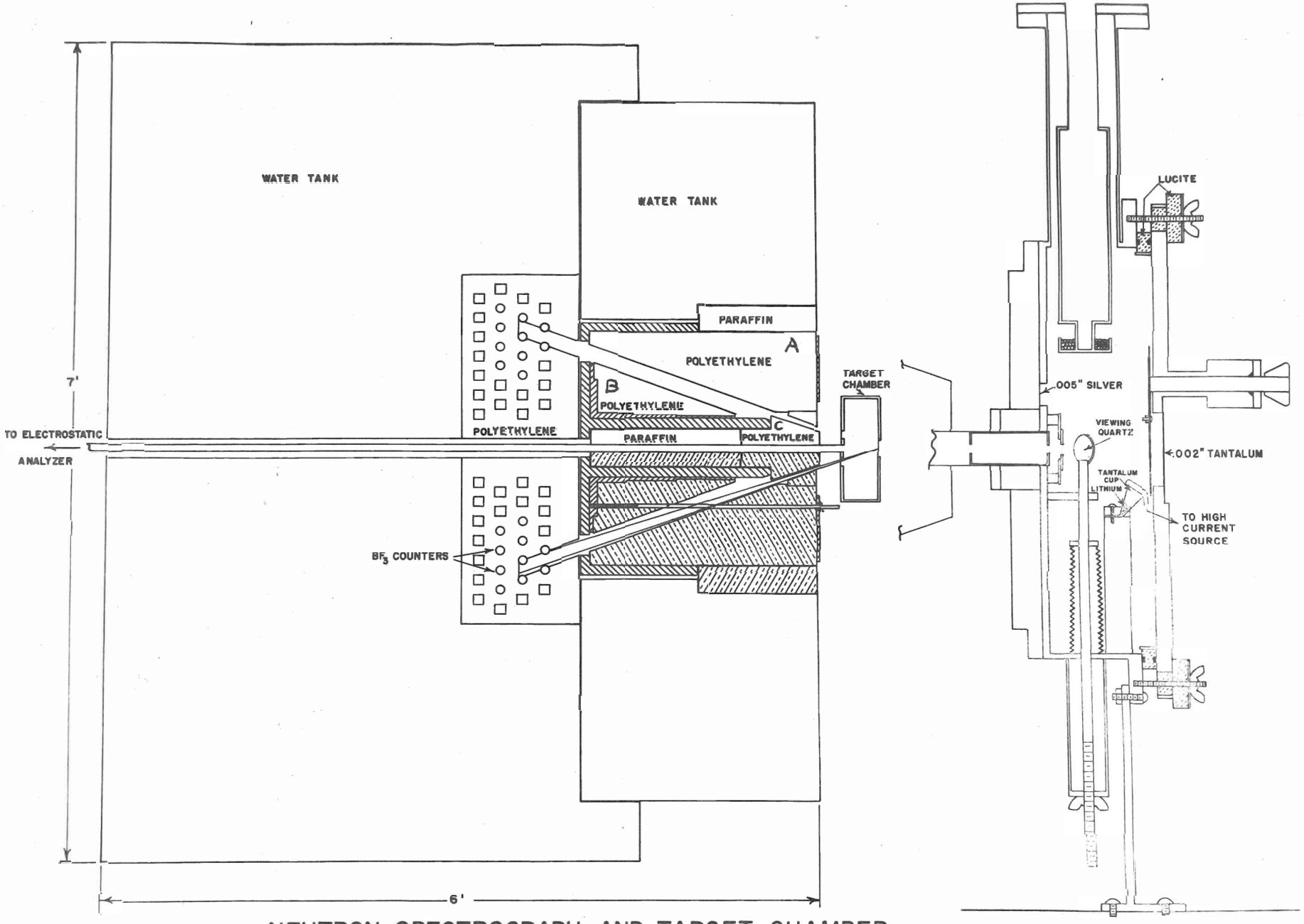

NEUTRON SPECTROGRAPH AND TARGET CHAMBER

Figure 2. Top View of Spectrometer and Side View of Target Chamber

(Cone B, Figure 2) has a male outer conical surface and a cylindrical inner surface and may be moved back and forth along a cast iron cylinder by turning rods which are threaded into the liner of the male cone and which are mounted on the stationary front plate on the first cone. Thus, the cone may be moved in such a manner as to open or close the acceptance angle for the neutrons to any size desired between 0° and 2°. (An opening of 4° is actually possible but has not been used in these experiments.) This conical geometry is used because the neutron energy is a function only of the latitudinal angle and not the azimuthal angle. Such an arrangement coupled with the adjustable opening yields advantages in both intensity and resolving power which will be discussed later. The iron cylinder surrounds and is coaxial with the beam tube carrying the protons to the Li target. This center cylinder is an integral part of the cast iron box which holds the outer cone in position and maintains the coaxial alignment of the instrument. The cylinder does not extend all the way to the front of the female conical surface of the first cone, and a third polyethylene cone or plug (Cone C, Figure 2) is placed rigidly in the end of this cylinder and maintains the fixed maximum opening of 1° in this front section of the spectrometer. Thus the opening is variable between 0° and 1° along most of the collimating surface and is fixed at 1° only in the front. The target chamber is mounted at the end of the beam tube in such a position that the lithium target is just inside the focus of the conical opening. The cast iron box with the cylindrical center which holds all three cones in place is supported by a cast iron

table encased in a steel water tank for shielding purposes (see Figure 3). This entire assembly is mounted upon jacks which rest upon a steel plate and may be moved by the use of lead screws in such a manner as to facilitate aligning the axis of the instrument with the proton beam. This entire unit is surrounded by a large water tank of an inverted "U" shape for shielding purposes (see Figure 4). The counter matrix detects the neutrons coming through the apertures which have been set to yield the desired angular opening. The counter matrix consists of an assembly of polyethylene strips and sheets which define spaces into which boron trifluoride counters have been inserted vertically. The counters are placed alternately between 1 inch square vertical polyethylene strips. Each such layer is separated from the succeeding one by a solid 1 inch thick polyethylene sheet. There are no counters within 6 inches of either side of the beam tube so that the neutrons entering either the left or the right side of the spectrometer will be counted separately with a negligible count of "cross-over" neutrons. Conical openings corresponding to the maximum $\Delta\theta$ used are cut through the cast iron supporting box back to the mid-point of the counter matrix to facilitate efficient counting of the neutrons. All of the counters in the left bank are connected in parallel and the output goes through a pre-amplifier, linear amplifier, pulse height discriminator and into a scalar-printing recorder combination. The circuitry for the right bank is identical. The counting efficiency for the banks has been estimated at twenty per cent. The instrument is completed by the addition of a very large

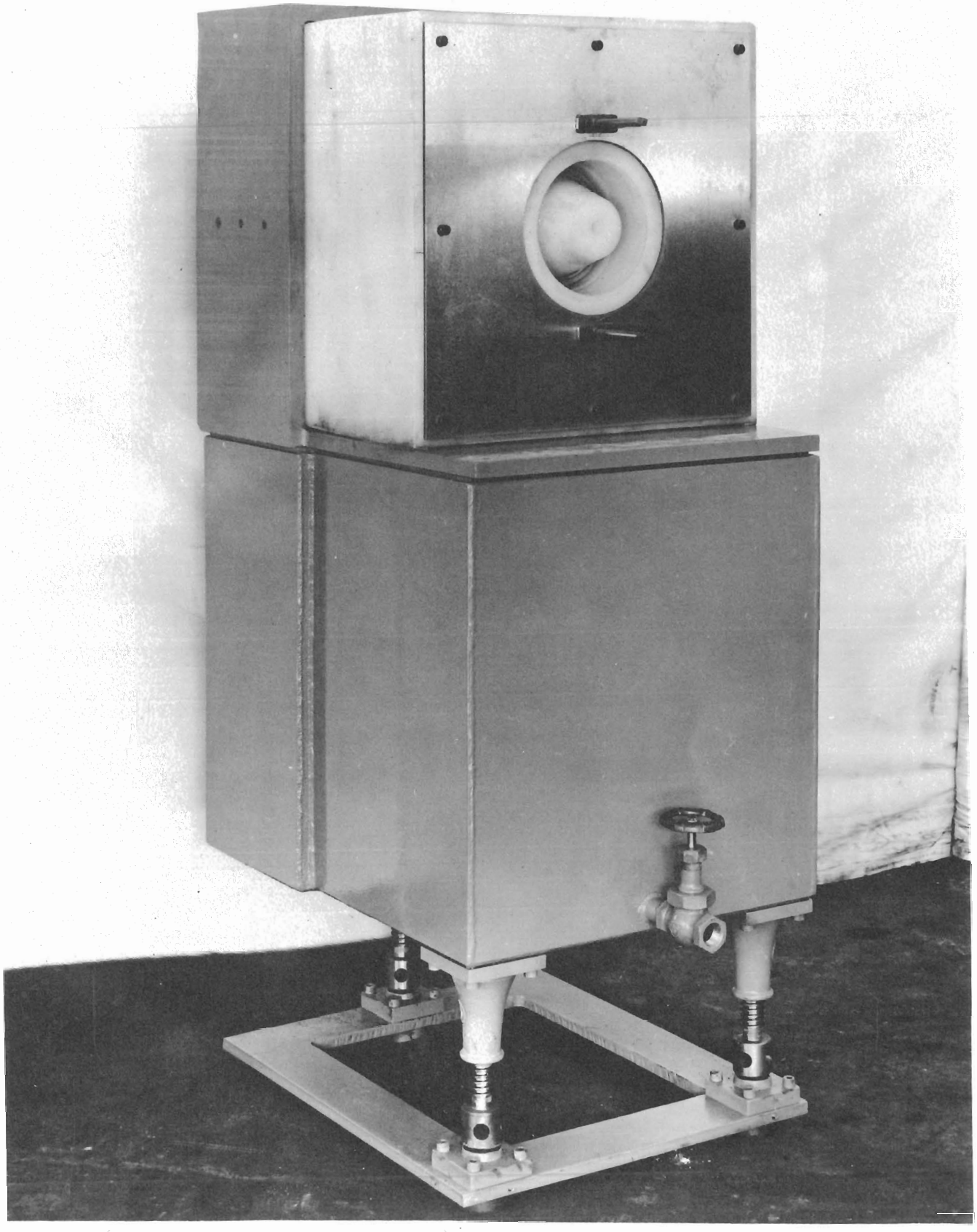

Figure 3. The Unshielded Spectrometer

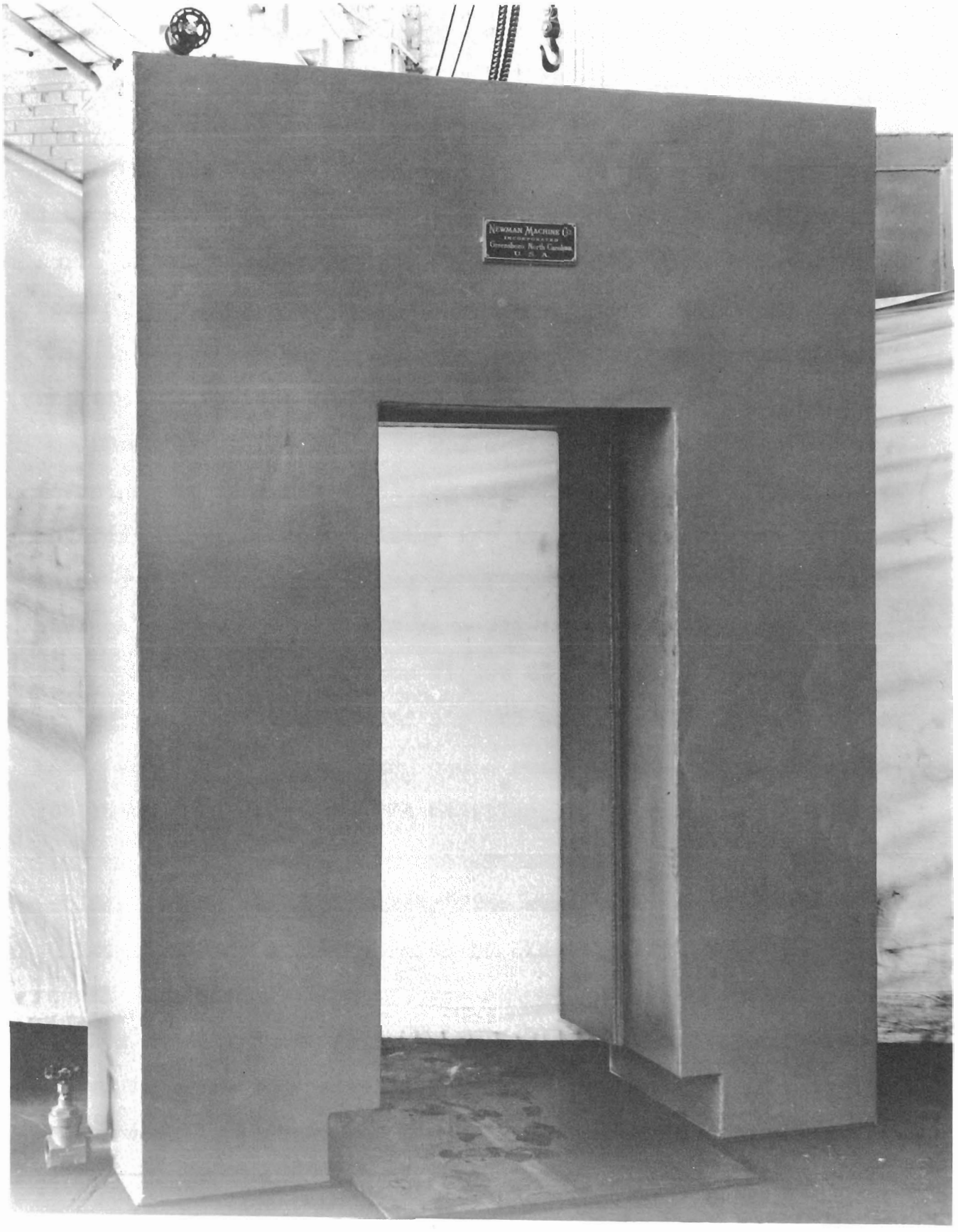

Figure 4. The Forward Shielding Tank

water tank, the front of which rests against the back of the counter matrix, and the sides of which join and lap over the large inverted "U"-shaped tank, and by the addition of shielding above the top of the counter matrix so that it will detect a minimum number of neutrons scattered from the ceiling and other parts of the laboratory (see Figure 5). The whole instrument is carefully constructed to include steps between adjoining parts so that the neutrons have no direct path through the small spaces between the various components of the structure.

Before the spectrometer was designed an experiment was performed to measure the shielding effect of water as a function of neutron energy. The shielding for the spectrometer was made thick enough so that the number of neutrons reaching the detectors through the shielding would be negligible up to about 500 kev.

The target chamber (see Figure 2) consists of a brass exterior, a combination liquid air and activated charcoal trap, an internal lithium evaporator, and a rotating disk to which a target shutter is attached. In addition, there are quartz observation windows, tantalum beam collimating disks, and a quartz target for visual beam alignment. The evaporator is composed of a conical tantalum crucible which is electrically heated by an external high current, low voltage source. The cone is filled with lithium and aimed at the tantalum target backing. The front plate, on which the target is mounted, is insulated from the rest of the target chamber by a lucite ring so that a correcting voltage up to 10 kv may be applied (see Chapter III). In order to maintain a high vacuum, neoprene gaskets and other materials

Figure 5. Assembly of Major Spectrometer Components

which might outgas have been held to a minimum and metal-to-metal seals with indium and lead "O" rings have been used wherever possible. The windows in the back plate through which the neutrons pass into the angular openings in the spectrometer are of .005 inch silver. Care was taken in the design to reduce backscatter into the counters from scattering materials in the target chamber to a minimum. Two remote-controlled sample mounts were constructed to swing the half-circular samples alternately into the path of neutrons entering the left and right banks of counters. This permitted a convenient measurement of two different sample thicknesses at the same neutron energy.

Chapter III

DESIGN CONSIDERATIONS

Let us discuss some of the problems which were considered in the design of the instrument previously described, and how these problems were treated.

In order to obtain high resolving power, one must reduce all of the factors contributing to the spread, or smear, in the neutron energy distribution to a minimum. However, the intensity of the neutron flux actually reaching the neutron detectors, or counters, must be kept at a high enough level to make possible a reasonable speed in making the measurements.

The factors contributing to a finite width of the neutron energy distribution are the initial width of the proton distribution from the cylindrical electrostatic analyzer,[7] the thickness of the lithium target used to produce neutrons from the Li(p,n)Be reaction, the width of the angular latitudinal opening in the spectrometer which admits neutrons to the counters, the

finite size of the beam spot, and finally the inhomogeniety introduced by the Doppler motion of the lithium atoms in the lithium target. We shall now consider each component of the final spread separately.

The width of the proton distribution, ΔE_p, has been reduced from that used in previous neutron total cross section measurements made in this laboratory. This has been accomplished by a modification[8] of the cylindrical electrostatic analyzer[7] which not only increases the resolving power, but in addition improves the emerging proton intensity. This modification, referred to as the homogenizer, largely compensates for time variations of the energy of the proton beam coming from the Van de Graaff and the analyzing magnet. In this arrangement the entire constant negative deflecting voltage is applied to the inner plate of the cylindrical analyzer and a small correction voltage, v, which compensates for the time variations is impressed on the outer plate. The error signal for this compensating voltage is obtained from insulated exit slits on the analyzer. The effect is to make a larger portion of the beam emerge since the time required for the protons to pass through the analyzer is short, and the compensating voltage is applied rapidly. The remaining problem is to compensate for the departure of the energy of the emerging proton beam from the energy corresponding to the potential difference between the inner plate and ground. This is done by imposing a voltage upon the insulated lithium target which is the proper multiple of the compensating voltage to cancel the energy shift permitted by that compensating voltage. In

practice a potentiometer is connected between the source of the target voltage and ground, and the appropriate fraction is fed back to the outer plate of the analyzer. The homogenizer power supply cannot actually produce a negative voltage, so the plate and target voltages are impressed upon a positive bias of several kilovolts. The result is a proton beam of better resolution and higher intensity. In principle, one can obtain either very good intensity or very good resolution with the analyzer alone by opening or closing the slits, but not such a favorable combination of both. The spread caused by inhomogeniety of the proton beam is reduced by the homogenizer to such an extent that it is effectively negligible.

The lithium target must be of great enough thickness to provide sufficient neutron intensity, but also as thin as possible so that the protons will not be slowed down too much as they pass through the target and introduce a large spread in the neutron distribution. A neutron produced at the face of the target will have a greater energy than one produced near the back of the target where the proton has been slowed down somewhat by ionization. Let us define the neutron spread in the final distribution caused by finite target thickness alone as $\Delta L = (\partial E_N/\partial E_p)\Delta S$ where ΔS is the thickness of the target in proton stopping power. If the lithium target is exposed to the atmosphere between the time of evaporation and proton bombardment, the lithium oxidizes very rapidly and increases the stopping power of the target layer. Such target oxidization is greatly reduced by evaporating the lithium within the target chamber where a good vacuum is always

maintained.

The energy of the neutrons from the Li(p,n)Be reaction is a function of the latitudinal angle θ measured from the incident proton direction in the lab system. A finite opening, $\Delta\theta_l$, into the counters is mandatory to obtain a useable neutron intensity, but we wish to keep the opening as small as possible because ΔE_N increases with the angular opening $\Delta\theta_l$.

Now an angle θ of less than $\pi/2$ is not desirable because in this case we have two neutron groups for $E_N < 118$ kv. A back angle is the obvious choice, and since $\partial E_N/\partial\theta$ decreases with increasing θ, and vanishes at $\theta = \pi$, a choice of angle close to π is desirable. However, if the angle is too close to π, the detectors must be placed too close to the beam tube where they may count neutrons which did not enter through the collimator. It also becomes difficult to separate the counters into two separate banks which will count neutrons on the left and right side of the spectrometer independently without counting neutrons which diffuse from one side of the matrix to the other. The angle of 160° is a good compromise and was selected for this equipment.

At low neutron energies ($E_N \approx 5$ kv) it is not difficult to obtain relatively good resolution, because $\partial E_N/\partial E_p$ and $\partial E_N/\partial\theta$ are small. However the yield at the back angles (see Figure 8, Chapter IV) is small for such a low neutron energy, and it is desirable to be able to increase the angular opening $\Delta\theta_l$, to increase the intensity. Conversely, at higher energies of 80 kv to 100 kv, the intensity is better by almost an order of magnitude and is less of a problem, but $\partial E_N/\partial\theta$ increases quite rapidly

and becomes the predominant part of the final neutron energy distribution width. Thus one also wishes to be able to decrease $\Delta\theta_1$ for the measurements at higher energies. Hence it was decided to make $\Delta\theta_1$ mechanically variable.

The beam spot must have a finite size, and this also introduces a spread in the resultant neutron energy. The beam spot has a diameter of d and this corresponds to an angle of $\Delta\theta_2$. This diameter is 1/8 inch and a further decrease results in too great a loss in proton intensity.

The spread in the resultant neutron distribution due to Doppler effect in the lithium target alone, ΔD, is not a variable parameter if the target is operated near room temperature.

Let us consider more carefully how the various spreads combine. We must make appropriate assumptions concerning the shapes of the component distributions, and then select the correct weighting factor for each. We shall assume that the target and Doppler distributions with widths at half maximum of ΔL and ΔD are Gaussian in shape. The two angular spreads of width ΔA and ΔS are rectangular in shape. $\Delta A = (\partial E_N/\partial\theta)\Delta\theta_1$ and $\Delta S = (\partial E_N/\partial\theta)\Delta\theta_2$. Now if several rectangular distributions are combined, the result is very close to a Gaussian. Therefore, we may assume that if two rectangular distributions and two Gaussian distributions of roughly comparable widths are all combined, the result is reasonably close to a Gaussian.

Let us first see how several Gaussian functions of unit area unite. If λ_i are the standard deviations of the Gaussians, the standard deviation, λ_R, when they are joined is expressed

by:

$$\lambda_R = \left[\sum_1 \lambda_1^2\right]^{1/2} .$$

This formula holds exactly only for Gaussian distributions, and in order to use the expression, we must replace the two rectangular distributions with equivalent Gaussians.[9] Let us assume that two distributions with the same area and same standard deviation are equivalent. The standard deviation of the distribution which results when two Gaussians and two rectangular distributions are combined is given with a reasonable degree of accuracy by

$$\lambda_R = \left[\lambda_1^2 + \lambda_2^2 + \lambda_3^2 + \lambda_4^2\right]^{1/2} .$$

The width at half maximum for a Gaussian is 2.36λ, and we have

$2.36\lambda_R = \left[(2.36\lambda_1)^2+(2.36\lambda_2)^2+(2.36\lambda_3)^2+(2.36\lambda_4)^2\right]^{1/2}$ where each term is now a width at half maximum, or the square of that width. Let us now return to the case at hand. We may write the expression above as follows:

$\Delta E_N = \left[(\Delta D)^2+(\Delta L)^2+(.681\Delta A)^2+(.681\Delta S)^2\right]^{1/2}$. Figure 6 is a plot of ΔE_N, the width of the resultant Gaussian spread, ΔD, the width of the Gaussian Doppler spread, ΔL, the width of the lithium target spread, ΔA, the width of the rectangular angular spread, and ΔS, the width of the rectangular finite beam spot spread. (When the component spreads are combined to form the resultant, the two rectangular component widths must be multiplied by $2.36/2\sqrt{3}$ because $2.36\lambda_3 = (2.36/2\sqrt{3})\Delta A = .681\Delta A$, and

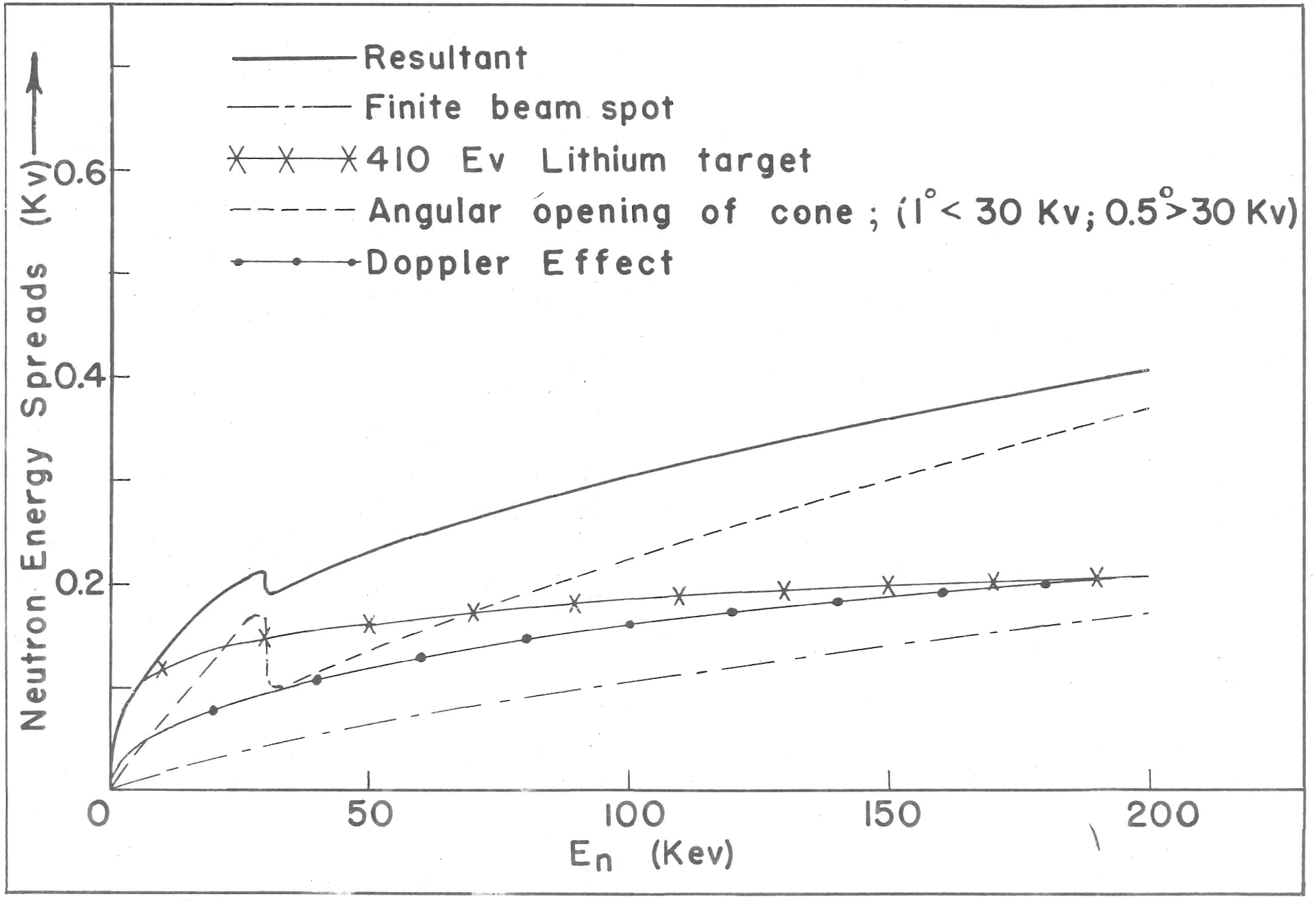

Figure 6. Calculated Resolution as a Function of Neutron Energy

$2.36\lambda_4 = .681\Delta S$. This is the case since the standard deviation of a unit rectangle is the width of the rectangle divided by $2\sqrt{3}$. If there were a triangular component of width ΔX at half maximum, a term $(0.963\Delta X)^2$ would occur in the expression for ΔE_N.)

The angular opening and target thickness must be of sufficient magnitude to obtain a useable neutron intensity. It obviously does not help the resolution appreciably to reduce one spread when another is predominating. With these considerations in mind, the actual values selected for ΔL, ΔA, ΔS, and ΔD are the smallest which will still yield a reasonable counting rate. The target thickness is selected to approximately match the Doppler spread at an energy of 200 kilovolts. An angular opening of 1.0° is used below 30 kv, and an opening of 0.5° is used above 30 kv.

Chapter IV

GENERAL EXPERIMENTAL PROCEDURE

The spectrometer must be carefully aligned before the experiment can be started. The axis of the spectrometer must coincide with the beam to avoid an unnecessary angular energy spread. A circular beam limiting aperture is placed inside the beam tube at the rear face of the polyethylene cones. A forward aperture in the target chamber is also in position. The spectrometer is then adjusted so that the beam clears both apertures and the axial alignment is ensured.

The next step is to evaporate a lithium target of the desired thickness. A fresh, clean tantalum target backing is mounted in place on the target chamber, and the chamber is sealed and evacuated. Next the activated charcoal in the base of the liquid air trap is outgassed by placing an electric heating element down the inside of the trap and heating the charcoal sufficiently to release adsorbed gasses; the lithium in the tantalum

crucible is then melted to obtain a clean surface on the lithium. The target shutter is held in place over the tantalum backing so that no lithium will be deposited on the target. Liquid air is placed in the trap to improve the vacuum and make the charcoal effective as a "getter". The lithium is again heated several more times with the shutter still in place over the target until the vacuum does not become too much worse with mild heating (very slight reddening) of the tantalum cone. The shutter is removed and the current is increased to a point at which the cone becomes a medium dull red and lithium is deposited on the target backing for a very short time (perhaps one second). The beam is then allowed to strike the target and a trial count is made for a given integrated proton current to estimate the thickness of the target. If the target is too thin, the procedure is repeated until a target of the desired thickness is obtained. The best vacuum obtainable is desirable during and after the target evaporation so that the target will not become contaminated. The target backing is cooled with a fine distilled water spray to which a household detergent has been added. The use of distilled water prevents the formation of deposits on the target backing, and the detergent tends to eliminate water droplets and insure a thin film of cooling water. Water droplets and thicker water films provide more material for the backscatter of neutrons into the counters and cause an increase in the undesirable heteroenergetic neutron background, and a $CaCO_3$ deposit from tap water spoils heat transfer.

Before any data is taken, an energy calibration must be made.

A neutron monitor similar to a McKibben Counter[10] is placed in front of the lithium target and a forward threshold for the Li(p,n)Be reaction is taken. The setting on the type k potentiometer[7] is proportional to the proton energy. The potentiometer setting at which the threshold occurs corresponds to a proton energy of 1.8814 Mev. This energy is the threshold for the Li(p,n)Be reaction. The neutron energy is a function of the proton energy, and is obtained from a plot of E_N vs. E_p at 160°. The potentiometer must be rebalanced frequently. Any accumulation of carbon or oxygen deposits on the lithium target will alter the energy calibration, but a target becomes unserviceable and is discarded before an energy shift becomes important.

The measurement actually made in this laboratory is a determination of the transmission ratios for samples of various thicknesses of the element under study at appropriate neutron energies over the range of interest. The samples are prepared in the form of semicircular cylindrical rings of constant thickness in a direction normal to that of neutron incidence. The samples are mounted in such a fashion that one sample shadows one bank of counters and the other is clear of the neutron flux into the other bank. The count is started and continued until a given number of counts is recorded from the latter bank. Both the shadowed (or "in") count and the unshadowed (or "out") count is recorded. The positions of the samples are then so changed from the control console that the second bank is shadowed by a sample and the first is unshadowed. The transmission ratios obtained are then averaged to eliminate any differences in counting

efficiency between the two banks.

Two sample thicknesses are actually used over the energy range of a resonance. This permits the use of the double difference method[11] which is discussed in Appendix C and an application of the peak height method discussed in Appendix D. Both methods utilize the data for both thicknesses. An automatic recorder[12] which plots (1-T) while each point is being taken is connected in parallel with the scalar-printer which is taking the "in" count. This permits an observation of the (1-T) curve without further computations while the experiment is in progress. This curve is later utilized in conjunction with the tapes from the scalar-printer combination in making a finished plot of the data.

The resolution is checked occasionally by repeating the measurement of a narrow resonance which has been run previously under good conditions. If the resolution has become poor, the evaporation of a new target, balancing of the homogenizer, or other corrective action is in order.

Chapter V

THE EXPERIMENTAL DATA

The bismuth samples were prepared from metallic bismuth with a purity of 99.8%. The metal was cast to slightly more than the desired thickness in a cylindrical die with an outer diameter of ~4-1/16 inches and an inner diameter of ~2-1/8 inches. The samples were then machined to the desired thicknesses from the castings. Each casting was cut along a diameter to form two separate samples so that one could be used to shadow each counter bank. Samples of the following thicknesses were used in this experiment:

$N_1 = 0.532 \times 10^{+23}$ atoms/cm^2

$N_2 = 0.266 \times 10^{+23}$ atoms/cm^2

$N_3 = 0.133 \times 10^{+23}$ atoms/cm^2

Between ~10 kev and ~30 kev, the experiment was performed over the entire range with samples of thickness N_2, and the resonances alone in that region were also measured simultaneously with

samples of thickness $N_3 = N_2/2$. The availability of data taken with two sample thicknesses made possible the double difference and peak height analysis.[11] (See Appendices C and D.) In the region between 30 kev and 135 kev, the samples used for the lower energy region are too thin because the maximum value of the cross section decreases with increasing energy, and the values of the transmission ratio T, where $T = \exp(-N\sigma)$ would be too large. With this consideration in mind, samples of thickness N_1 were used in the higher energy region. Once again samples of half this thickness were used at the resonances. Longer counts were taken with both thicknesses at the resonance peaks to reduce the statistical uncertainty of the measurement. See Appendix B for a discussion of this consideration. The transmission ratio was measured at intervals of about one-fourth of a neutron kilovolt where there were resonances or suspected resonances, and at larger intervals in the regions that seemed to have no structure. The cone opening used for energies less than 30 kev was one degree. Above 30 kev this opening was decreased to one-half of one degree, because the energy spread introduced by the angular collimation opening increases more rapidly with energy than do the other spreads.

Figure 7 shows the experimental bismuth data. σ and 1-T are plotted versus neutron energy. The first curve shows 1-T and σ from 10 kev to 35 kev for samples of thickness N_2 and the lower three curves are for thickness N_1 from 30 kev to 137 kev. The statistical probable error is slightly less than the size of the experimental points in Figure 8 at the resonance peaks, and

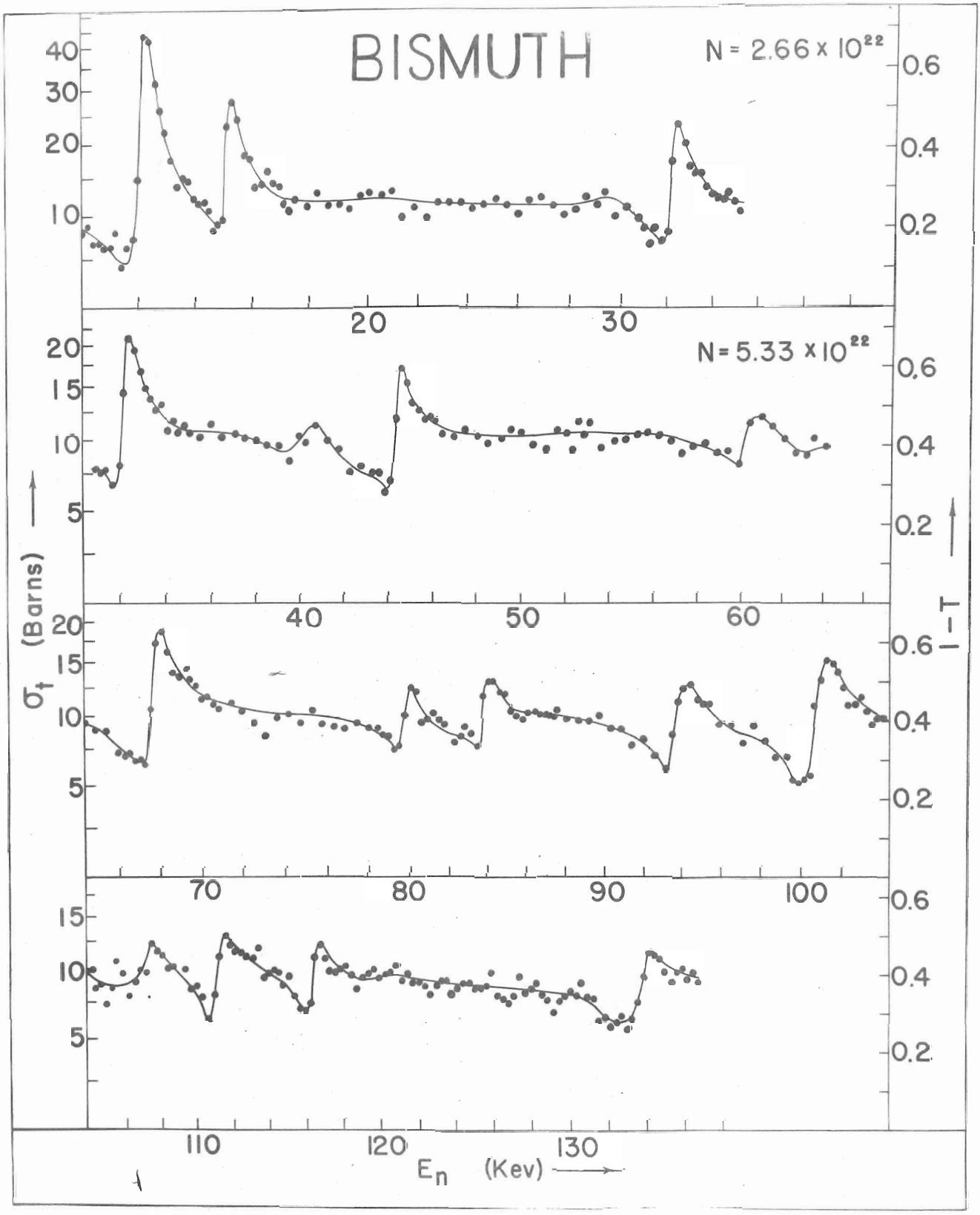

Figure 7. The Bismuth Data

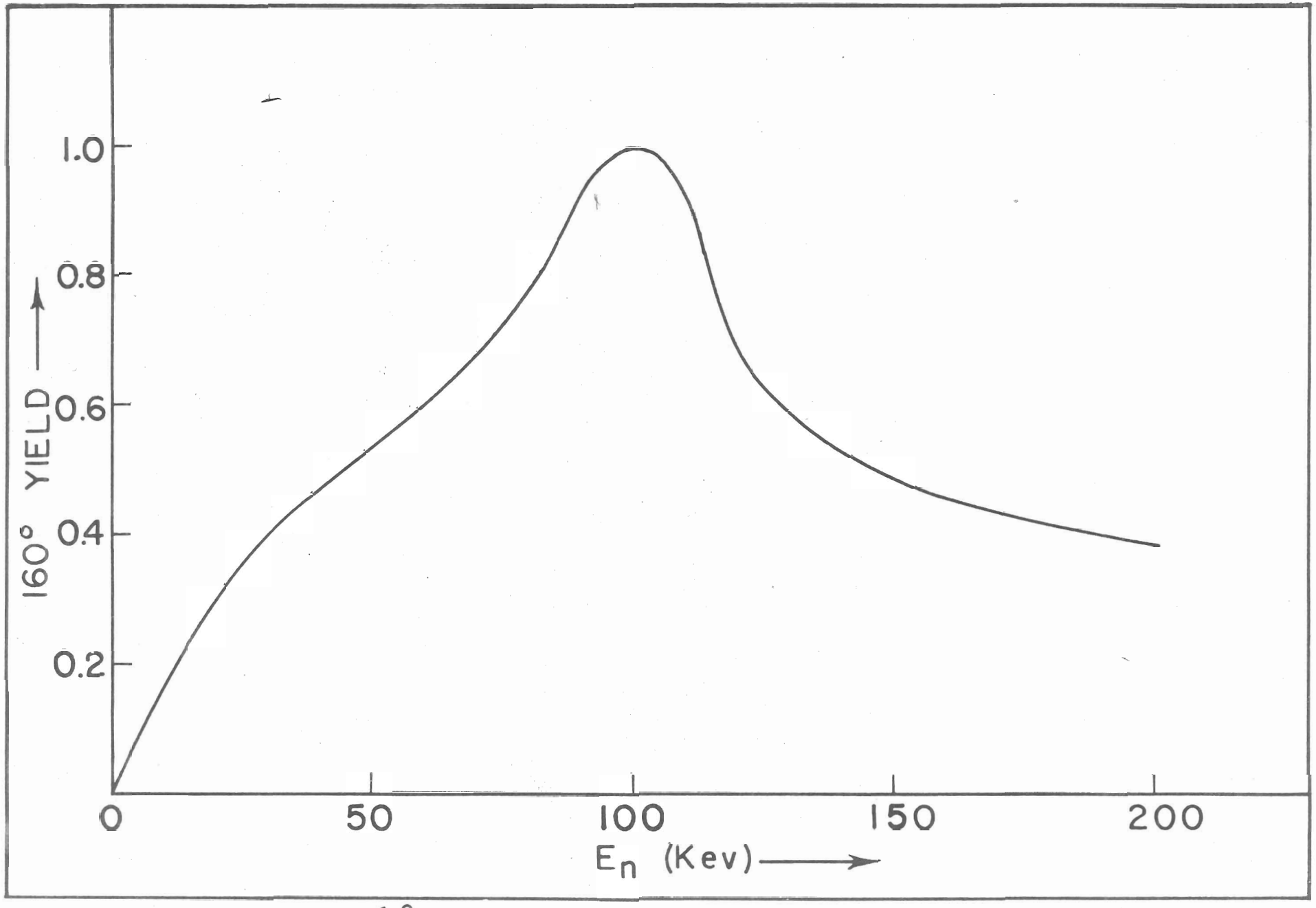

Figure 8. The 160° Yield Curve

slightly greater than the size of the points elsewhere.

The intensity detected by the counters as a function of neutron energy at 160° has also been measured. The experiment was performed using the same target throughout the run, and the angular opening between the cones was fixed at a constant value of 1°. Figure 8 shows a plot of the yield normalized to unity at its maximum value at about 100 kev.

The background, which consists of neutrons whose energy is considerably different from those in the primary neutron energy distribution, has also been measured. The technique is to select wide levels in various nuclei which can be completely resolved, and to use samples of sufficient thickness that most resonant neutrons are scattered. The intensity detected by the counters in the process of an "in count" consists then primarily of "off energy" or background neutrons.

Let us now see how the background is computed from this data. We shall assume that the transmission ratio which would have been measured in the absence of background is (I/I_o). We actually measure (I'/I'_o), where

$$\frac{I'}{I'_o} = \frac{I + \alpha I_o e^{-N\bar{\sigma}}}{I_o + \alpha I_o} = \frac{I/I_o + \alpha e^{-N\bar{\sigma}}}{1 + \alpha} \quad .$$

Now $k = \alpha/(1 + \alpha)$ is the fraction of the measured "out count" which is due to background, and $\bar{\sigma}$ is the average cross section for the energy range of neutrons constituting the background. Now if the resonance is completely resolved, $I/I_o = e^{-N\sigma_{Max}}$ where $\sigma_{max} = g4\pi\chi^2 + (1 - g)\sigma_{pot}$ (see Appendix A). (If the

sample is thick enough, $I/I_o = 0$.) We now make the assumption that the background is caused by forward angle neutrons which are scattered back into the detector by the tantalum backing of the lithium target and by other scattering materials in the forward portion of the target chamber. We then estimate $\bar{\sigma}$ for the appropriate neutron energy range. Since α is nearly proportional to the measured "in count", I', a correction for the small counter background is important here and must be made. A plot of k, the background fraction versus neutron energy is shown in Figure 9. The true background is not so large as indicated by this measurement. The resonances are not wide enough so that the finite width of the incident neutron distribution actually becomes negligible. The measured background decreases when the resolution spread is further reduced. However, the counting rate diminishes too much to make possible measurements of the wide resonances with optimum resolving power. The elements used for the measurement were iron at 28 kev, fluorine at 50 kev, aluminum at 92 kev, fluorine at 99 kev, and calcium at 134 and 170 kev. The background fraction rises somewhat more sharply than would be expected above 100 kev. This may be caused by a scattering resonance in the cooling water oxygen, and/or backscattered protons striking lithium and producing off energy neutrons which then enter the detector.

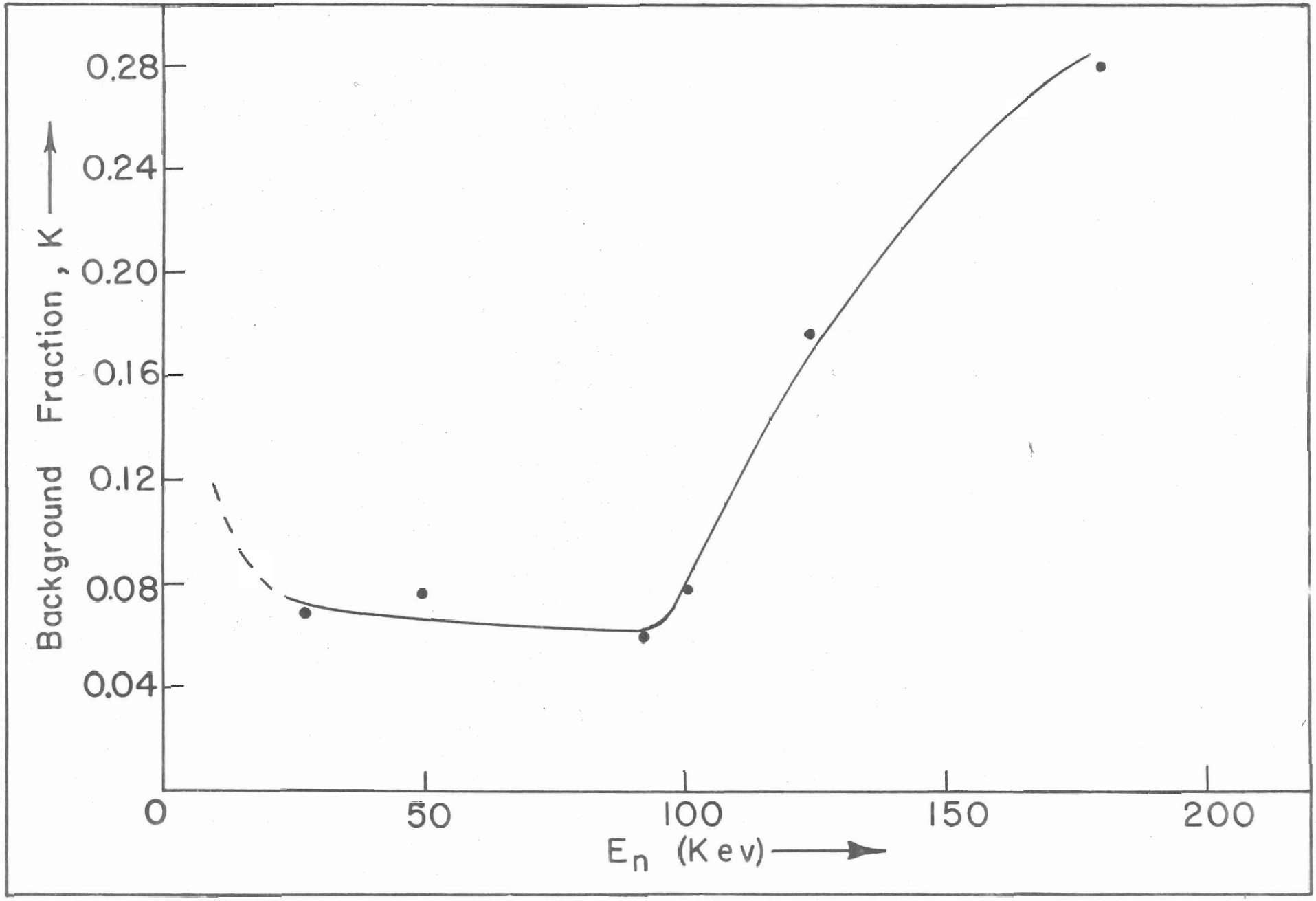

Figure 9. The Background Fraction

Chapter VI

RESULTS AND CONCLUSIONS

Bismuth exhibits relatively prominent resonances at 12, 15, 33, 45, 68, 80, 84, 94, 101, 112, 117, and 134 kev in the energy region between 10 and 136 kev. There is also good evidence of levels at 61 kev and 108 kev and there is apparently a comparatively narrow resonance at 41 kev. Narrow resonances may be present at 106 kev and 131 kev. Any other levels that may occur are too narrow to be indicated with the present resolution.

Of the prominent resonances listed above, those above 50 kev are almost resolved in the sense that nearly their true shape is measured. They have been corrected for background using the background fraction data which is shown in Figure 9. The corrected transmission ratio, T, is related to the measured transmission ratio, T', by the expression

$$T' = (T + \alpha e^{-N\bar{\sigma}})/1 + \alpha$$

where $\bar{\sigma}$ is the average cross section for the background neutrons, $\alpha = k/(1 - k)$, and k is the background fraction. Then we have

$$T = \exp(-N\sigma_{Max})$$

where σ_{Max} is the sum of the maximum value of the resonance cross section and the potential cross section for the non-resonant channel (see Appendix A). In general we are unable to make a positive distinction between the two possible g values ($g_1 = 9/20$ and $g_2 = 11/20$) for the level so we let $g = 1/2$ in the expression for the non-resonant channel potential cross section. We then have

$$\sigma_{o_{exp}} = \sigma_{Max} - 1/2(4\pi\lambda^2 \sin^2 kR')$$

where $\sigma_{o_{exp}}$ is the experimental resonance peak cross section. The values of $\sigma_{o_{exp}}$ are plotted on Figure 10 with solid dots. The solid curves represent the value of σ_{oth}, the theoretical resonance peak cross section for $J = 4$ and $J = 5$. The values of $\sigma_{o_{exp}}$ are also plotted with solid dots for the resonances at 12 kev, 15 kev, 33 kev, and 45 kev. For these resonances, however, σ_{Max} was not corrected for background to emphasize the increase in cross section obtained with the peak height method discussed in the next paragraph. The application of the background correction increases the value of σ_{exp} by 10b, 4b, 1b, and 1b respectively for the four resonances.

The peak height method of analysis[11] outlined in Appendix D was used on the four resonances below 50 kev. This method essentially corrects the apparent cross section for resolution

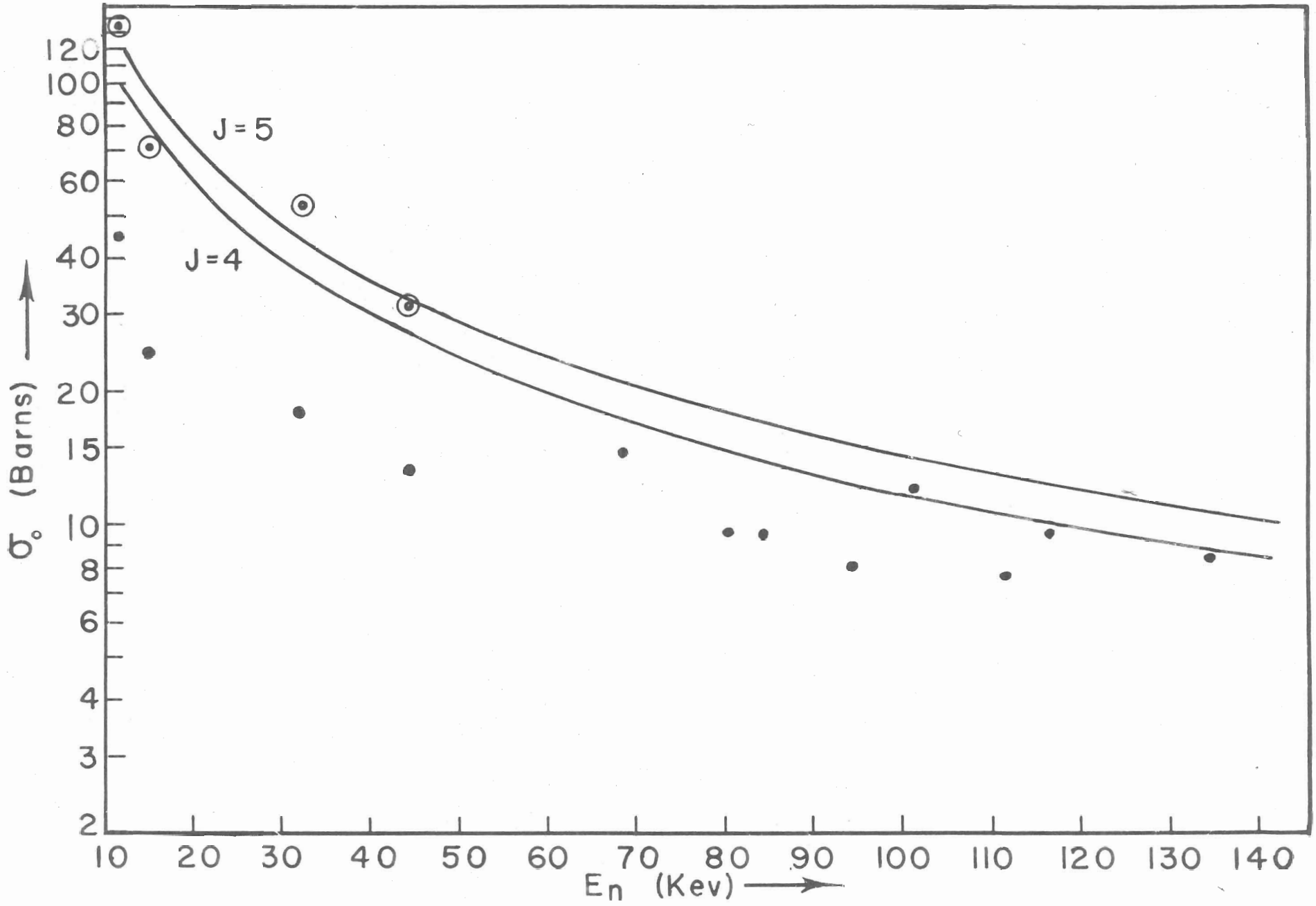

Figure 10. $\sigma_{o_{exp}}$ and $\sigma_{o_{th}}$ vs. E_N

and we compare the values obtained with $\sigma_{o_{th}}$, the theoretical resonance peak cross section. The method is rather insensitive to the presence of a background because the background is pretty well absorbed in the resolution correction. The results of the peak height analysis are plotted in Figure 10 with circled dots. It is probable that the 12 kev and the 33 kev resonances are $J = 5$ levels, and the 15 kev level is probably a $J = 4$ level. The 45 kev level is doubtful in J assignment as are the higher energy resonances. The two possible $\ell = 0$ statistical weight factors, $g_1 = 9/20$ and $g_2 = 11/20$ corresponding to the angular momenta $J = 4$ and $J = 5$ of the bismuth levels are so close that it is difficult to assign the J value of the levels. This is the case because the two values of σ_o corresponding to g_1 and g_2 are proportional to the appropriate g. However, if there is more difference between the two g values as is often the case (the high spin of the bismuth nuclei causes the g values to be so close), it should be relatively simple in many cases to make a positive determination of the J value for a resonance.

The width, Γ, has been computed assuming $g = 1/2$ from the area analysis discussed in Appendix E. The values have been corrected for the effect of the interference term, using the thin sample approximation listed in that appendix. On the next page is a table of the uncorrected widths, the factor K by which the width must be multiplied to correct for the interference term, and the corrected widths and reduced widths. The values of Γ obtained are merely estimates, and even the widths listed for the resonances below 70 kev are probably correct to within only a

The Bismuth Widths

E_N (kev)	Γ_n (ev) (uncorrected)	K	Γ_n (ev) (corrected)	Γ_n^o (ev) (corrected)
12	137	1.28	175	1.59
15	116	1.32	154	1.25
33	70	1.85	130	.72
45	104	2.22	231	1.04
68	282	3.03	855	3.27
80	38	3.85	146	.52
84	178	4.17	736	2.53
94	127	5.26	664	2.16
101	244	6.66	1620	5.08
112	136	10.0	1360	4.07
117	59	12.5	737	2.15
134	87	-500.	-	-

factor of 2. The error introduced from the proper selection of the local potential scatter level and the determination of the actual area is relatively large and increases with energy in this region. The interference correction is also obviously not perfectly correct. The correction factor K is discontinuous for an energy of about 130 kev. Physically, this means that the expected area measured on the transmission curve vanishes for a resonance at this energy when the approximations of Appendix E are used. For energies somewhat higher than 130 kev, the area is negative if the thin sample prediction is exactly valid and K also becomes negative. The area measured for the 134 kev resonance was

positive but quite small and there was a considerable margin of error in making the measurement. Another method of determining Γ for resonances of such asymmetry is needed.

The double difference cross section discussed in Appendix C is sometimes good enough to determine the value of J for a resonance without any further corrections if the g values differ sufficiently. An additional resolution correction can be made to the double difference cross section if the resolution and the width are known. This is a further aid in determining J values in some cases. However, the widths of the bismuth resonances are uncertain and this method cannot be applied effectively. The double difference cross sections were not significantly higher than the experimental cross sections for the resonances above 35 kev. The double difference cross sections for the three resonances below 35 kev are about 25% higher than the cross section measured for the thinner of the two samples.

The level spacing observed in the energy region between 10 kev and 135 kev is about 16 kev for each J value, assuming that we have an equal number of $J = 4$ and $J = 5$ levels . The value quoted by Gibbons[13] is 20 kev. The 122° spectrometer constructed earlier in this laboratory was used for that data.

A comparison of the resolution of the 122° spectrometer and the new 160° spectrometer reported in this thesis is of interest. The peak height method of analysis was used on both the new data (see Figure 7) and the old data[14] ($N = .282 \times 10^{23}$) for the 12 kev resonance. Z and β were used to determine α for each and the ratio of the two α's yielded the improvement in resolution.

The analysis indicates that the width of the resolution function for the 160° spectrometer is 59% of the width present under good conditions for the 122° spectrometer. The corresponding factor is about 20% at 200 kev.

Because of the extreme interference distortion of the bismuth resonances, it is difficult to make a reasonably accurate determination of the resolution function which was actually present when the resonances were measured. However, data[12] has been taken with the spectrometer herein described on aluminum, calcium, barium, and strontium, and a better estimate of the resolution function can be made from the narrower and more symmetric levels in these elements. This estimate has been made using a variation of the peak height analysis in which one uses the experimental value of Z and an assumed β to obtain a value of the parameter α. Now $\alpha = 2.36\Gamma/2\sqrt{2}\ E_N$ and if a reasonably accurate determination of Γ can be made from the area analysis, ΔE_N, the half width of the resolution function, may be computed. The width of the resolution function may also be estimated[12] from the width of the 1 - T curve if Γ is known. There is some indication that the finite lithium target thickness is the predominant component of the resolution width because the values of ΔE_N obtained above seem to have about the same variation with energy as the target thickness spread. The target thicknesses were determined from the neutron yield under standard conditions, and it is quite likely that the thickness is somewhat greater with respect to its contribution to the resolution spread than it is with respect to yield. This would be the case if the Li were not deposited on

the tantalum by the evaporation process in a uniform layer, but instead adhered in grains or tiny globules. It is possible that the resolution was better during the measurement of the bismuth cross section than it was during the runs on strontium, barium, and calcium; and it was probably no worse. The lithium target used on the bismuth data had a thickness of about 600 ev (proton ev) as determined from yield considerations.

Resolution is considerably improved with this instrument, and the prospect for the assignment of many previously undetermined resonance parameters is good.

The resolution can be further improved by a greater reduction in the component spreads. Further work remains to be done in the technique of lithium target evaporation to obtain a thinner and more uniform layer. A more intense proton beam would make possible the use of still thinner lithium targets and smaller angular openings without sacrificing too much in counting rate.

A further reduction in background by minimizing the scattering material in the vicinity of the neutron source, and eliminating the possibility of neutron production by back-scattered protons would also be of considerable value in obtaining more accurate cross section measurements.

In conclusion it might be stated that the measurements made with this spectrometer, although gratifying, can still be considerably improved both in principle and in practice; and future refinements and development work remain to be done.

APPENDICES

APPENDIX A

BREIT-WIGNER SINGLE LEVEL FORMULA

The following is a brief derivation of the Breit-Wigner single level formula slightly modified from the treatment in Blatt and Weisskopf, Theoretical Nuclear Physics. We shall first consider the case of target nucleus spin equal to zero and later modify the results for $I \neq 0$. We represent the incident neutron beam first by an undisturbed plane wave expanded into spherical harmonics in which only the $\ell = 0$ term is retained:

$$e^{ikz} \approx \frac{i}{2kr}\left[e^{-ikr} - e^{ikr}\right] \tag{1A}$$

for large kr where k is the incident de Broglie wave number.

The interaction changes this expression in that the outgoing wave is altered.

$$\psi(r) \approx \frac{i}{2kr}\left[e^{-ikr} - \eta_o\, e^{ikr}\right] \tag{2A}$$

where η_o is the coefficient of the outgoing wave. The scattered

wave is given by:

$$\psi_{Sc}(r) = \psi(r) - e^{ikz}$$

$$= \frac{i}{2kr}\left[1 - \eta_o\right] e^{ikr} \qquad (3A)$$

Then the number of neutrons scattered is expressed by

$$N_{Sc} = \frac{\hbar}{2iM}\int\left(\frac{\partial\psi_{Sc}}{\partial r}\psi^*_{Sc} - \frac{\partial\psi^*_{Sc}}{\partial r}\psi_{Sc}\right) dA$$

$$= \frac{v\pi}{k^2}\left|1 - \eta_o\right|^2 \qquad (4A)$$

The incident number of neutrons /cm^2/sec is

$$N = v \qquad (5A)$$

where v is the velocity. We then define the scattering cross section

$$\sigma_{Sc} = \frac{N_{Sc}}{N} = \pi\lambda^2\left|1 - \eta_o\right|^2 \qquad (6A)$$

Now let us assume the existence of a well defined nuclear radius R, and consider the behavior of the wave function for smaller values of r down to r = R.

Now we can describe the relative motion of the nucleus and the neutron with no interaction between them by:

$$\nabla^2\psi(r) + k^2\psi(r) = 0 \qquad (7A)$$

We let $\psi(r) = u_o(r)/2\sqrt{\pi}r$ and substitute this expression in the wave equation to obtain a differential equation for u,

$$\frac{d^2u_o(r)}{dr^2} + k^2u_o(r) = 0 \qquad (8A)$$

which has as a general solution

$$u_o(r) = ae^{-ikr} + be^{ikr} \qquad (9A)$$

Comparing this with the first expression for ψ which is valid for large kr, we evaluate the constants and obtain

$$u_o(r) = \frac{i\sqrt{\pi}}{k}\left[e^{-ikr} - \eta_o\, e^{ikr}\right] \qquad (10A)$$

We now relate η_o with the conditions at the nuclear surface and define

$$f_o \equiv R\left[\frac{du_o(r)/dr}{u_o(r)}\right]_{r=R} \qquad (11A)$$

Substituting the last expression for $u_o(r)$ in f_o, we obtain for η_o:

$$\eta_o = \frac{f_o + ikR}{f_o - ikR}\, e^{-2ikr} \qquad (12A)$$

Using this expression in the formula for σ_{Sc}, we have

$$\sigma_{Sc} = \pi\lambda^2\left|\frac{-2ikR}{f_o - ikR} + e^{2ikr} - 1\right|^2 \qquad (13A)$$

We may define:

$$A_{res} = \frac{-2ikR}{f_o - ikR} \text{ and } A_{pot} = e^{2ikR} - 1 \qquad (14A)$$

Now at resonance, $|A_{res}|$ is large and this implies a value of f_o close to zero. We expand f_o around the resonance energy E_o and retain only the first term

$$f_o(E) = \left(\frac{df_o}{dE}\right)_{E=E_o} (E - E_o) \tag{15A}$$

We now define Γ, the half width of $|A_{res}|$, as

$$\Gamma = -2kR/\left(\frac{df_o}{dE}\right)_{E=E_o} \tag{16A}$$

Now we obtain the following:

$$A_{res} = \frac{i\Gamma}{(E - E_o) + i\Gamma/2} \tag{17A}$$

Then

$$\sigma_{Sc} = \pi\lambda^2 \left| \left(\frac{i\Gamma}{(E - E_o) + i\Gamma/2}\right) + (e^{2ikR} - 1)\right|^2 \tag{18A}$$

If $I \neq 0$ ($I = 9/2$ for bismuth), the only change is that the expression above is multiplied by the statistical weight factor g_1 for the resonant channel and an additional term is added to represent the contribution to the potential scattering from the non-resonant channel, and we have finally

$$\sigma_{Sc} = g_1\pi\lambda^2 \left| A_{res} + A_{pot}\right|^2 + g_2\pi\lambda^2 \left| A_{pot}\right|^2 \tag{19A}$$

A_{res} and A_{pot} are unchanged from the expressions stated above. Since $g_2 = 1 - g_1$, we may write

$$\sigma_{Sc} = g_1\pi\lambda^2 \left| A_{res} + A_{pot}\right|^2 + (1 - g_1)\pi\lambda^2 \left| A_{pot}\right|^2 \tag{20A}$$

A_{res} and A_{pot} interfere destructively for $E < E_o$ and result in a minimum in cross section for an energy slightly lower than the resonant energy. $\sigma_{max} - \sigma_{min} = g4\pi\lambda^2$.

Feshback, Porter and Weisskopf[16] have pointed out that

R should be replaced by R' which differs appreciably from R. R' is constant on the average, but the local value of R' is dependent upon neighboring levels.

APPENDIX B

STATISTICAL UNCERTAINTIES

Let us consider the statistical uncertainties[17] introduced by taking a finite count of events in determining a measurement instead of the infinite count which would be required to make the measurement accurately.

If a count N is taken of events which occur at a steady but random rate for a finite period of time, a discrepancy will occur between that count and the average count N_o that would be measured for that time if the actual measurement were continued infinitely. If one made a large number of measurements of the count N for a finite period of time, and a plot were made of the number of times the count N occurred versus the value of the count, a Poisson distribution centered on the value N_o would be the result.

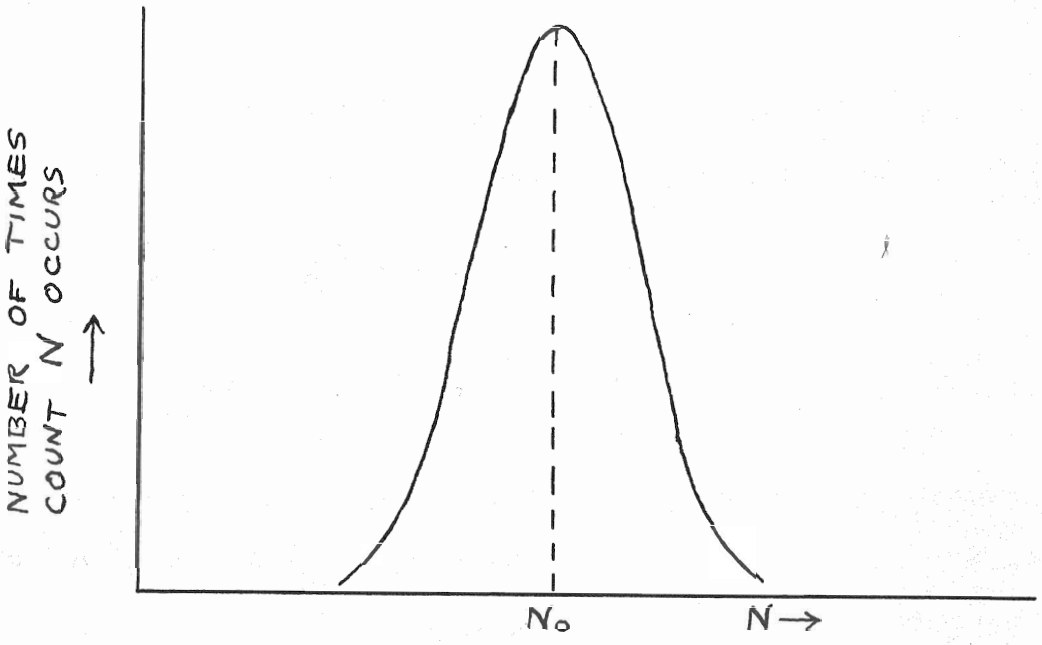

The probability that any given count N will fall within $\pm \Delta N$ of N_o depends upon the magnitude of N, and our selection of ΔN.

If we wish to select ΔN as the standard deviation, the probability that a single measurement will fall within $\pm \Delta N$ of N_o is 0.68, where

$$\Delta N = N^{1/2} \qquad (1B)$$

If we now wish to make a measurement of N as a function of another parameter, we may construct limits of ΔN on that count and say that the probability that the count is within ΔN of the exact value N_o is 0.68.

In this research a measurement is made of a transmission ratio, or the ratio of an "in" count to an "out" count, both of which contain such statistical variations, and we wish to construct limits of $\pm \Delta T$ upon the measured transmission ratio T, such that there is a certain probability that the measured value with occurs/in $\pm \Delta T$ of the exact ratio T_o that could only be obtained

by running the experiment for an infinite length of time with a finite counting rate. In this case ΔT is determined as follows:

$$T \pm \Delta T = \left(\frac{I}{I_o}\right) \pm \Delta\left(\frac{I}{I_o}\right) \text{ where}$$

$$\Delta\left(\frac{I}{I_o}\right) = \left[\left(\frac{\Delta I}{I}\right)^2 + \left(\frac{\Delta I_o}{I_o}\right)^2\right]^{1/2} \left(\frac{I}{I_o}\right) \tag{2B}$$

If we again select ΔT as the standard deviation, the probability is again 0.68, and $\Delta \frac{I}{I_o}$ becomes

$$\Delta\left(\frac{I}{I_o}\right) = \left[\frac{1}{I} + \frac{1}{I_o}\right]^{1/2} \left(\frac{I}{I_o}\right) \quad \text{since } \Delta I = I^{1/2} \tag{3B}$$

The probable error which is as likely to be exceeded as not exceeded (a probability of 0.50) is the product of 0.6745 and the standard deviation, or

$$\Delta\left(\frac{I}{I_o}\right)' = 0.6745 \left[\frac{1}{I} + \frac{1}{I_o}\right]^{1/2} \left(\frac{I}{I_o}\right) \tag{4B}$$

Error bars on data in this dissertation represent the probable error.

APPENDIX C

SAMPLE THICKNESSES AND THE DOUBLE DIFFERENCE METHOD

The proper selection of sample thickness is essential in obtaining the best possible measurement of the total scattering cross section by the transmission ratio method using this instrument.

The apparent cross section σ_t is expressed as follows: $I/I_o = e^{-N\sigma t}$ where I, I_o, N, and σ_t are the "in" and "out" counts, the sample thickness in nuclei per square centimeter, and the cross section in barns, for neutrons of an energy E_N.

Now the neutron flux into the detectors contains a number of neutrons with an energy other than E_N. Part of this off-energy component results from neutrons scattered into the counters from scatterers such as the ceiling, walls, and floor of the laboratory, some of the shielding near the conical openings into the detectors, portions of the sample itself and any other objects in the vicinity. Most of the remainder of the neutrons

with energy different from E_N reaching the counters are from the sides of the neutron distribution, or energies slightly higher or lower than the nominal energy. Now the expression above for the cross section indicates an exponential decrease of the neutron intensity through the sample for neutrons on any energy, but since $\sigma_t = \sigma_t(E_N)$, the expression for the transmission ratio becomes:

$$\frac{I}{I_o} = e^{-N\sigma_t(E_{N_o})} \; e^{-N\sum_i \sigma_t(E_{N_i})} \qquad (1C)$$

when neutrons of energy other than E_{N_o} are present. If we are at a nominal neutron energy which is well off resonance and the cross section is relatively flat, this has little effect upon the measurements, but if we are at a resonant energy and the sample is too thick, virtually all of the neutrons of resonant energy will be scattered within a short distance into the sample, and the exponential expression will not be very valid for the cross section at resonance energy. Most of the neutrons traversing the entire sample thickness will be slightly "off-energy" or background neutrons. For this reason, it is desirable to use a sample thin enough at resonance so that an appreciable number of neutrons of resonant energy can still penetrate the sample and the exponential expression is still reasonably valid at that energy. However, by using samples of various thicknesses greater than this, one is able to make an estimate of the background by comparing the results with those obtained with the thinner samples.

If a sample of insufficient thickness, or small N, is used the statistics become very bad and the expression for the uncertainty $\Delta\sigma$ becomes too large because it is inversely proportional

to N.

$$\Delta\sigma = \frac{0.6745}{N}\left[\frac{1}{I} + \frac{1}{I_o}\right]^{1/2} \qquad (2C)$$

(See Appendix B).

A measurement of a resonance with two different sample thicknesses is also of value in effectively increasing the resolution.[11] A choice of two relatively thin samples which differ in thickness by a factor of 2 is made. Let us consider the neutron energy distribution which is centered upon the resonant energy E_o. If no sample shadows the detectors, it counts the entire distribution. Now if a thin sample of thickness N_1 shadows the detector, practically all the neutrons pass through the sample and are counted except for some of the neutrons of resonant energy and those very close to resonant energy for which the cross section is much higher than the "off-energy" neutrons. If a sample of thickness N_2 where $N_2 = 2N_1$ is now placed in the neutron beam, the neutrons scattered are still primarily resonant neutrons, or have energy very close to resonance, as long as the second sample is still thin enough so that a fairly large portion of resonant neutrons and practically all the off-energy neutrons can still pass through the sample. Let us denote the count with no sample in position by I_o, the count with the sample of thickness N_1 in position by I_1 and the count with the second sample of thickness N_1 in position behind the first by I_2, all for a given number of neutrons from the lithium target. Then $I_o - I_1$ is the number of resonant or near resonant neutrons scattered by a sample of thickness N_1 alone and $I_1 - I_2$ is the

number scattered by the second sample of thickness N_1 behind the first.

Let us consider the expression

$$1/T_D = \frac{I_o - I_1}{I_1 - I_2} = \frac{1 - I_1/I_o}{I_1/I_o - I_2/I_o} \tag{3C}$$

now $I_1/I_o = e^{-N_1\sigma}$ and $I_2/I_o = e^{-N_2\sigma}$. Then

$$\frac{1}{T_D} = \frac{1 - e^{-N_1\sigma}}{e^{-N_1\sigma} - e^{-N_2\sigma}} \tag{4C}$$

But $N_2 = 2N_1$, so

$$\frac{1}{T_D} = \frac{1 - e^{-N_1\sigma}}{e^{-N_1\sigma} - e^{-2N_1\sigma}} = \frac{1 - e^{-N_1\sigma}}{e^{-N_1\sigma}(1-e^{-N_1\sigma})} = e^{N_1\sigma} \tag{5C}$$

or

$$\sigma = \frac{1}{N_1} \ln \frac{1}{T_D} = \frac{1}{N_1} \ln \frac{1 - I_1/I_o}{I_1/I_o - I_2/I_o} \tag{6C}$$

where I_1/I_o is the transmission ratio for a sample of thickness N_1 and I_2/I_o is the transmission ratio for a sample of thickness $N_2 = 2N_1$.

This method effectively increases the resolving power at resonance because only the resonant or near resonant neutrons denoted by $(I_o - I_1)$ and $(I_1 - I_2)$ are used in the computation. The peak cross sections determined in this manner for the bismuth data were higher than the apparent cross sections measured experimentally for the resonances at 12 kev, 15 kev, 33 kev, and 45 kev, and about the same for the prominent resonances at higher energies.

APPENDIX D

PEAK HEIGHT ANALYSIS

We shall briefly outline the peak height analysis. Dr. Eugen Merzbacher[11] has developed a family of curves relating β, α, and Z where

$$\beta = N\sigma_{res}$$

$$\alpha = 2.36\Gamma/2\sqrt{2}\Delta E_N$$

$$Z = \frac{T(E_o)}{\exp(-N\sigma_{pot})} = \frac{\int P(E_N, E_o)\exp(-N\sigma_{res})dE_N}{\int P(E_N, E_o)dE_N}$$

N = sample thickness in 10^{24} cm^2

ΔE_N = half width of $P(E_N, E_o)$

$P(E_N, E_o)$ = Gaussian neutron energy distribution

E_N = neutron energy

E_o = neutron energy at resonance

Γ = width of resonance occurring at E_o

$T(E_o)$ = transmission ratio at resonance

Z is plotted versus α for a number of different β's. Note that for simplicity the interference term has been neglected.

The analysis is utilized in a slightly different manner than has been used before in this laboratory. One measures the transmission ratio at resonance for two samples which differ in thickness by a factor of 2. Z is computed for each thickness by dividing the transmission ratio by $\exp(-N\sigma_{pot})$. A value of β is determined for each Z for a number of different α's and the ratio of β_2/β_1 is plotted versus α for each α selected. Now the resonance has a certain σ_{res} associated with it and the ratio of β_2/β_1 must be equal to 2 because the known sample thicknesses differ by that factor. To obtain the σ_{res} corresponding to the experimental Z's one merely finds the value of β_2 or β_1 where the plot of β_2/β_1 crosses the ordinate $\beta_2/\beta_1 = 2$. For example, $\beta_2 = N_2\sigma_{res}$ and we may immediately determine σ_{res} once β_2 is known. This method has been used on the resonances at 12 kev, 15 kev, 33 kev, and 45 kev. (See the discussion in Chapter VI and refer to Figure 10).

APPENDIX E

AREA ANALYSIS

An estimate of the width, Γ, of a resonance may be made by means of an area analysis.[15] The basic premise is that the area defined by

$$A_{meas} = \int_0^{\infty} (T_{pot} - T_{BW})\, dE \qquad (1E)$$

is independent of the resolution. $T_{pot} = \exp(-N\sigma_{pot})$ and $T_{BW} = \exp(-N\sigma_{BW})$ where σ_{BW} is the Breit Wigner expression for a resonance of width Γ at an energy E_o.

The following assumptions are made:

1) We may replace the limits on the integral above with $-\infty$ to $+\infty$ since the effect of a single resonance is small far from the resonant energy.

2) T_{pot} may be assumed constant over the energy range in which the area defined above is significant.

3) The interference term in the expression for σ_{BW} may be neglected for simplicity because to a first approximation it is an odd function about the resonant energy and the effects cancel.

The first two assumptions are quite good, but the third introduces some error, and an approximate correction will be indicated later in this appendix. Utilizing these three assumptions, we have

$$A = \int_{-\infty}^{\infty} \left[1 - \exp(-N\sigma_{pot} - N\sigma_{res})\right] dE \qquad (2E)$$

where $A = A_{meas}/T_{pot}$. After long computations we have

$$A = \frac{\pi\beta\Gamma}{2} e^{-\beta/2} \left[I_o(\beta/2) + I_1(\beta/2)\right] \qquad (3E)$$

$I_o(\beta/2)$ and $I_1(\beta/2)$ are Bessel Functions. Two cases may be explicitly evaluated:

for $\beta/2 << 1$, $A = \pi\beta\Gamma/2$

for $\beta/2 >> 1$, $A = \sqrt{\pi\beta}\,\Gamma$

For the intermediate case of $0.1 < \beta/2 < 10.0$, the full expression must be evaluated.

The quantity $y = \sqrt{\pi}\Gamma/A$ is plotted versus $\beta = N\sigma_o$. σ_o is the value of σ_{res} at the resonant energy E_o.

This plot is used in the following manner. The value of y is obtained from the plot for the possible values of β. A is determined from the experimental data using an energy interval $\pm\,\delta E$ from E_o. $2\,\delta E$ is selected such that it is much greater than the expected Γ. The value of y then yields the quantity Γ when A is known. A correction may be made once Γ is obtained for the area lost in using only the finite energy interval $2\delta E$ by the use

of the following expression for ΔA:

$$\Delta A = \frac{\beta \Gamma^2}{2 \delta E} \tag{4E}$$

Now $A' = A + \Delta A$ and a new Γ is obtained from the value of y using A' instead of A. This process may be repeated until there is no variation in A' and hence, in Γ. Note that the expression for A in integral form above contains no resolution correction, and none is needed as long as the original premise holds that the area is independent of the resolution.

Let us now consider the expression for A when the interference term is included.[18] The cases in which $\beta/2 << 1$ and $\beta/2 >> 1$ can be evaluated fairly easily, but the intermediate case is much more difficult. We will quote here the results of the calculation for the two simple cases.

1) $\beta/2 << 1$

$$A = \frac{\pi \beta \Gamma}{2} \left[\cos 2\alpha - (\beta/4)\sin^2 2\alpha\right] \tag{5E}$$

where $\alpha = kR'$. Let $K = \left[\cos 2\alpha - (\beta/4)\sin^2 2\alpha\right]^{-1}$. We multiply the Γ obtained from the area analysis by K to get the corrected Γ.

2) $\beta/2 >> 1$

We can place upper and lower limits on A as follows:

$$A > \sqrt{\pi\beta}\,\Gamma\left[\sqrt{\cos 2\alpha}\,(2 - e^{x^2/2y})\right] \tag{6E}$$

$$A < \sqrt{\pi\beta}\,\Gamma\left[\sqrt{\cos 2\alpha}\,(1 - x^2/2y)\right] \tag{7E}$$

where $x = \beta/2 \sin 2\alpha$ and $y = \beta/2 \cos 2\alpha$.

REFERENCES

REFERENCES

(1) Chadwick, J. Proc. Roy. Soc. London A136, 692 (1932).

(2) Bohr, N., Nature 137, 344 (1936).

(3) Breit, G., and E. P. Wigner, Phys. Rev. 49, 519 (1936).

(4) Fermi et al, Proc. Roy. Soc. A146, 483 (1934).

(5) Dunning, J. R., and G. B. Pegram, Phys. Rev. 43, 497 (1933).

(6) Blatt, J. M., and V. F. Weisskopf, Theoretical Nuclear Physics (John Wiley and Sons, New York, 1952).

(7) Toller, A. L., "Neutron Resonances in Sodium, Aluminum, and Potassium", Ph.D. thesis, Duke University, 1955.

(8) Parks, P. B., H. W. Newson, and R. M. Williamson, Bull. Am. Phys. Soc. Ser II, 3 (1958).

(9) Merzbacher, E., private communication.

(10) Hansen, A. O., and J. L. McKibben, Phys. Rev. 72, 673 (1947).

(11) Merzbacher, E., P. W. Crutchfield, Jr., and H. W. Newson, to be published.

(12) Bowman, C. D., Master's thesis, Duke University, 1958.

(13) Gibbons, J. H., Phys. Rev. 102, 1574 (1956).

(14) Marshak, H., "Neutron Resonances in Odd-Intermediate Nuclei", Ph.D. thesis, Duke University, 1956.

(15) Seidl et al, Phys. Rev. 95, 476 (1954).

(16) Feshbach, H., C. E. Porter, and V. F. Weisskopf, Phys. Rev. 96, 448 (1954)

(17) Evans, R. D., The Atomic Nucleus (McGraw Hill Book Co., New York, 1955).

(18) Seth, K. K., to be published.

BIOGRAPHICAL SKETCH OF

Paul Frothingham Nichols

(for Ph.D. Thesis)

Born:

October 16, 1931, Berkeley, California

Education:

College of William and Mary, B. S., 1953
Duke University, Ph. D. (Physics), 1958

Positions:

Research Assistant, Duke University, 1953-1957
Second Lieutenant, United States Army, 1957
Research Associate, Duke University, 1958

Publications:

Nichols, P. F., R. G. Smith, and H. W. Newson, Phys. Rev. 99, 621(A) (1955).

Gibbons, J. H., H. Marshak, R. M. Williamson, R. C. Mobley, J. R. Patterson, and P. F. Nichols, Phys. Rev. 105, 198 (1957).

Nichols, P. F., A. K. Furr, and H. W. Newson, Bull. Am. Phys. Soc. Ser II, 4, 218 (1957).

Nichols, P. F., E. G. Bilpuch, and H. W. Newson, Bull. Am. Phys. Soc. Ser II, 3 (1958).

Bilpuch, E. G., L. W. Weston, C. D. Bowman, A. K. Furr, P. F. Nichols, and H. W. Newson, Bull. Am. Phys. Soc. Ser II 3 (1958).

Memberships:

Sigma Xi
Phi Beta Kappa